

Test on the anchoring components of steel shear keys in precast shear walls

Shao-Dong Shen^{1a}, Peng Pan^{2b}, Wen-Feng Li^{*3}, Qi-Song Miao^{3c} and Run-Hua Gong^{1d}

¹Department of Civil Engineering, Tsinghua University, Beijing 100084, China

²Key Laboratory of Civil Engineering Safety and Durability of China Education Ministry, Tsinghua University, Beijing 100084, China

³Complex Structural Design Division, Beijing Institute of Architectural Design, Beijing 100045, China

(Received May 16, 2019, Revised July 29, 2019, Accepted August 8, 2019)

Abstract. Prefabricated reinforced-concrete shear walls are used extensively in building structures because they are convenient to construct and environmentally sustainable. To make large walls easier to transport, they are divided into smaller segments and then assembled at the construction site using a variety of connection methods. The present paper proposes a precast shear wall assembled using steel shear keys, wherein the shear keys are fixed on the embedded steel plates of adjacent wall segments by combined plug and fillet welding. The anchoring strength of shear keys is known to affect the mechanical properties of the wall segments. Loading tests were therefore performed to observe the behavior of precast shear wall specimens with different anchoring components for shear keys. The specimen with insufficient strength of anchoring components was found to have reduced stiffness and lateral resistance. Conversely, an extremely high anchoring strength led to a short-column effect at the base of the wall segments and low deformation ability. Finally, for practical engineering purposes, a design approach involving the safety coefficient of anchoring components for steel shear keys is suggested.

Keywords: prefabricated shear wall; quasi-static test; embedded components; anchoring strength

1. Introduction

Shear walls are the main structural components of a building that bear both vertical and lateral loads, including gravity, wind, and earthquake loads. Prefabricated shear walls have attracted much attention because they are convenient to use in construction processes. Specifically, wall segments can be prefabricated in factories and assembled on site, reducing both construction waste and noise. Precast shear wall structures are thus widely regarded as being ecofriendly (VanGeem 2006), saving on labor, consuming little energy in their manufacture (Boafo *et al.* 2016), and having high construction efficiency. Moreover, many building structures fitted with precast shear walls have performed well in large earthquakes over recent decades (Fintel 1977, Fintel 1995, Ghosh 1995, Scanlon *et al.* 1988). Prefabricated shear walls are thus extensively applied in practical engineering.

Limited by transport requirements, a monolithic wall typically has to be divided into smaller segments before being transported to the construction site for assembly. Jointing techniques for assembling the wall segments have thus been researched extensively.

As an example, unbonded post-tensioned (UPT) steel strands have been used widely in assembling reinforced

concrete (RC) wall segments (Sritharan *et al.* 2015), where the RC panels are anchored to the ground by steel strands and post-tensioning anchors. The post-tensioning force reduces the tensile stress transferred to concrete (Smith *et al.* 2007), and the wall segments are endowed with self-centering behaviors (Khaled *et al.* 1995). However, UPT precast shear wall systems have insufficient energy dissipation capacity owing to a large gap at the base (Zhu *et al.* 2018). Accordingly, Sritharan *et al.* (2015) proposed an O-shaped mild-steel connector that can be used to link wall panels horizontally, and specimens have exhibited stable energy dissipation in full-scale tests.

Besides UPT walls, the vertical bars of adjacent RC wall panels can be connected using grout-filled splice sleeves (Ameli *et al.* 2016, Henin *et al.* 2015, Haber *et al.* 2014, Lin *et al.* 2016, Ling *et al.* 2016, 2017), where steel bars are anchored to splice sleeves embedded in the RC panels, while post-cast layers filled with non-shrinkage mortar are set between upper and lower panels.

Another typical technique is to link wall segments using dry connections, where assembly can be achieved by welding or bolting with the help of embedded parts. Deng *et al.* (2017) proposed a precast shear wall horizontally assembled using H-shaped mild-steel connectors, where the connectors were set into the slots between the parallel RC wall segments and welded onto the embedded anchoring components, which were composed of steel plates and 25-mm-diameter bars. Guo *et al.* (2019) similarly designed a three-story precast shear wall structure, which was assembled using anchored rebar steel plates and high-strength bolts, and their test results validated the seismic behavior of this novel structure. Notably, researchers have focused mainly on the linking strength at the wall joints

*Corresponding author, Professor

E-mail: liwenfeng00@126.com

^a Ph.D. Candidate

^b Professor

^c Professor of Engineering

^d MSc Student

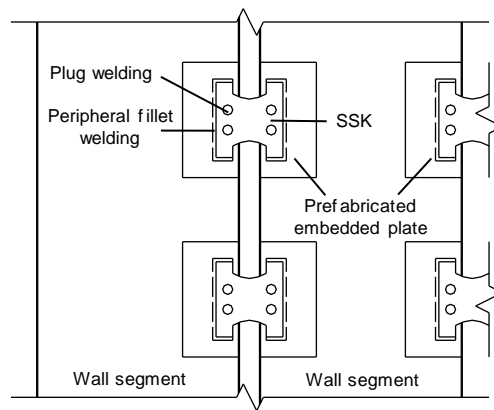


Fig. 1 Configuration of the SSKW

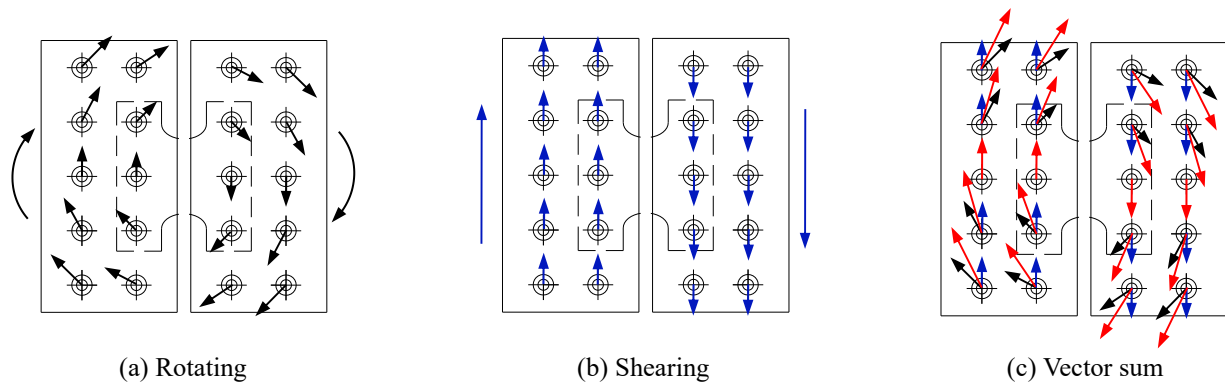


Fig. 2 Internal forces of embedded steel panels and rivets under the deformation of SSKs

instead of the anchoring strength of the embedded parts in the wall segments, which has been designed according to the checking equations for the relative specifications. However, the dimensions and strength of an embedded part affect the local stiffness and deformation ability of the RC wall segment and the mechanical properties of the entire precast shear wall, which are not considered in the checking equations.

The present paper proposes a precast shear wall assembled using steel shear keys (SSKW). As shown in Fig. 1, a typical SSKW is composed of wall segments, steel shear keys (SSKs), and embedded plates, where the SSKs are fixed on the embedded plates of the adjacent prefabricated wall segments by combined fillet and plug welding. The number and size of SSKs are to be specially designed to maximize the energy dissipation capacity under seismic loading (Shen *et al.* 2019a, b). Additionally, the embedded steel plate comprises a steel plate and rivets for anchoring. Two SSKW specimens with different anchoring components of shear keys were designed and loaded in quasi-static cyclic tests to develop a systematic design approach for anchoring components.

2. Design approach for anchoring components

In a typical SSKW, the internal forces of the wall segments are transferred by the SSKs to the anchoring components, which consist of embedded steel panels and rivets. Figs. 2(a) and 2(b) shows that, under the deformation of an SSK, the internal forces of the rivets on the embedded steel panels are made up of rotation and shear forces, and their design values depend on the in-plane shearing and flexural strength of the SSK. Thus, the designed internal forces of the rivets as shown in Fig. 2(c) were obtained by taking the sum of the vector forces shown in Figs. 2(a) and (b)

$$\vec{F}_{ri} = \vec{F}_{fi} + \vec{F}_{si} \quad (1)$$

where F_{ri} is the designed internal force of a rivet under the deformation of an SSK, F_{si} is the designed internal force of a rivet under in-plane rotation, which is obtained according to the ultimate flexural strength of the SSK, and F_{fi} is the designed internal force of a rivet under shearing, which is based on the ultimate shearing strength of the SSK.

Accordingly, the checking equation of a rivet is

$$n_s F_{ri} \leq N_{ri} (n_s \geq 1) \quad (2)$$

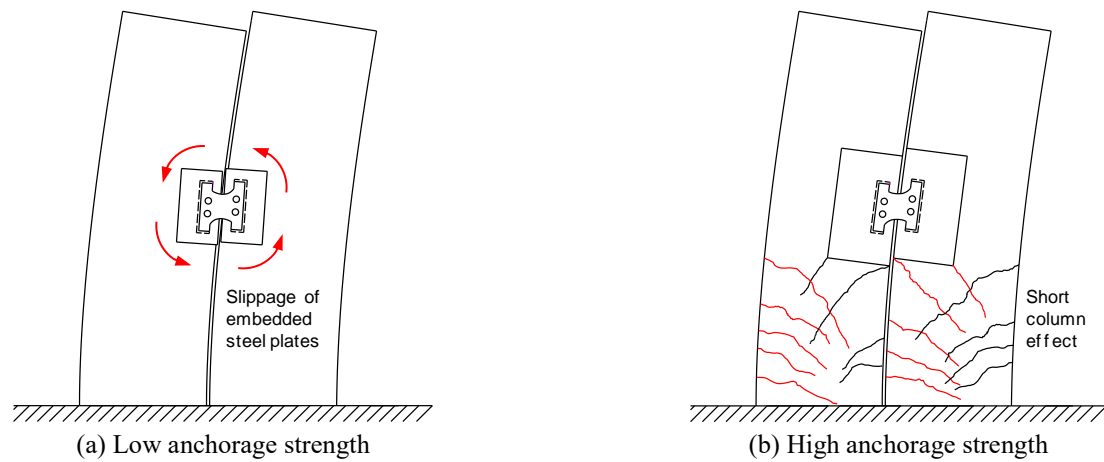


Fig.3 Shortcomings of precast shear walls with different anchorage strength

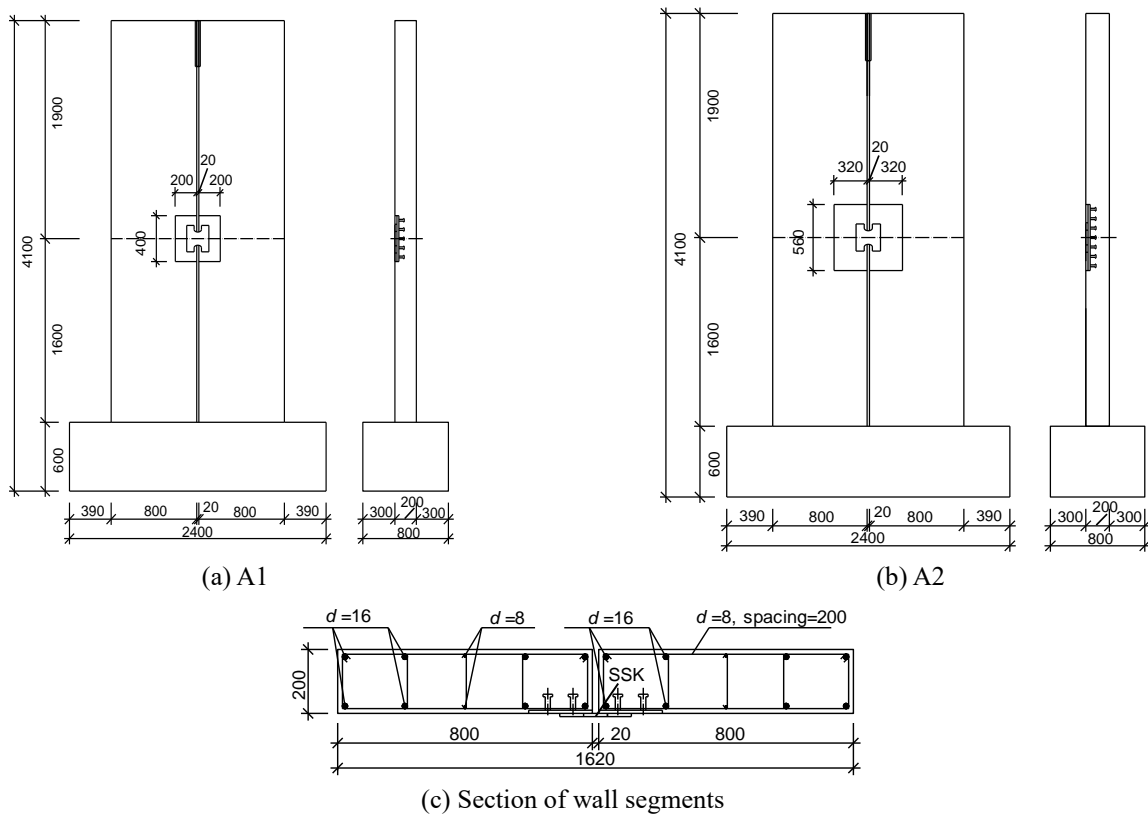


Fig. 4 Dimensions of test specimens

where N_{ri} is the bearing strength of a rivet (PRC National Standard, 2017), n_s is the safety coefficient, which is commonly no less than 1 such that the strength of a rivet is greater than the corresponding designed internal force.

However, owing to factors such as the construction quality and fatigue failure, if n_s is too small, the embedded steel panel with rivets provides insufficient anchoring strength. As shown in Fig. 3(a), under the lateral excitation of earthquakes, the embedded steel panels slip along with the shear keys owing to the fracturing of the rivets, which blocks the transference of the internal force between wall segments. Consequently, the wall segments function

independently absent of the effective linking provided by the SSKs. In contrast, if n_s is too large, the embedded panels need to be large and many rivets are required, as shown in Fig. 3(b). As a consequence, the wall segment is strengthened in the region of the anchoring components and a “short column” is produced between the embedded panel and the bottom of the shear wall, which exhibits a lack of deformation capacity and energy dissipation under seismic loadings. From another perspective, n_s also affects the stiffness of shear walls because it determines the dimensions of anchorage components, which directly affects the section stiffness of wall segments at the

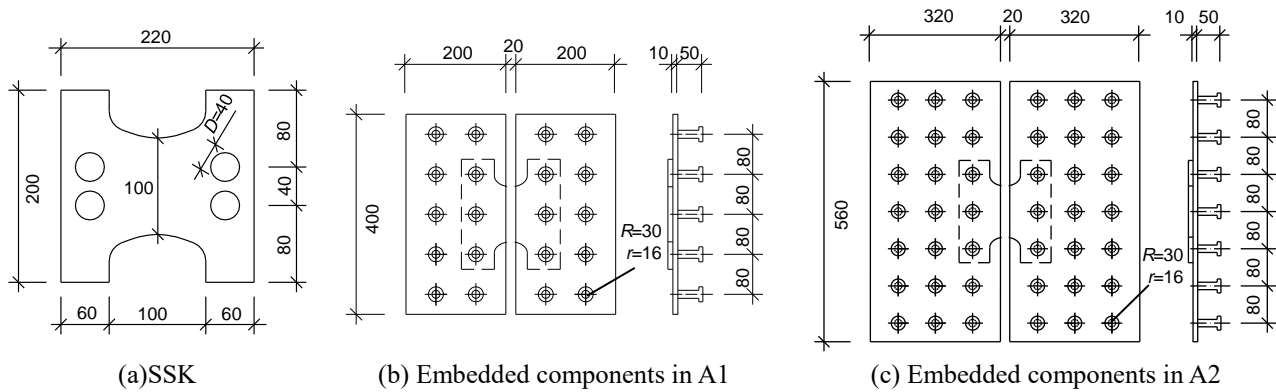


Fig. 5 Dimensions of SSKs and embedded steel panels

corresponding position. Thus, the mechanic properties of precast shear walls, including stiffness and deformation ability, are influenced by the safety coefficient n_s .

To this end, two specimens with different strengths of anchoring components of SSKs were designed to investigate the effects of the safety coefficient n_s on the seismic properties of SSKWs.

3. Quasistatic cyclic tests

3.1 Test specimens

Two SSKW specimens with the same dimensions, materials, and reinforcement were designed for loading, the only difference being the strength of anchoring components.

Figs. 4(a) and 4(b) shows that the two specimens, named A1 and A2, having a base block with dimensions of 2400 mm × 800 mm × 600 mm and shear wall with dimensions of 3500 mm × 1620 mm × 200 mm. A 20-mm vertical slot divides the shear wall into two identical segments and an SSK is welded to the anchoring components of the two wall segments, linking the wall segments together. As shown in Fig. 5(a), two specimens are fitted with the same SSK, and the dimensions of a SSK is determined according to the method proposed by El-Tawil (2010), which is aimed at controlling the relative strength between shear walls and connectors to obtain the best performance of shear walls.

The SSK anchorage components in A1 and A2, shown in Figs. 5(b) and 5(c), are named E1 and E2, where E1 comprises two 400 mm × 200 mm steel panels and a 4 × 5 array of rivets and E2 comprises two 320 mm × 560 mm steel panels and a 6 × 7 array of rivets. On the basis of formula (3), n_s values of E1 and E2 were designed to be 0.9 and 2.1, respectively.

In addition, the rebars of the specimens were made from HRB 400 steel bars and the SSKs were made from Q345 steel. The concrete, used for the wall segments and base beams, was C30. The results of material testing show that the average compressive strength of the C30 concrete was 41.8 MPa and the ultimate strength of HRB 400 rebar was 455 MPa.

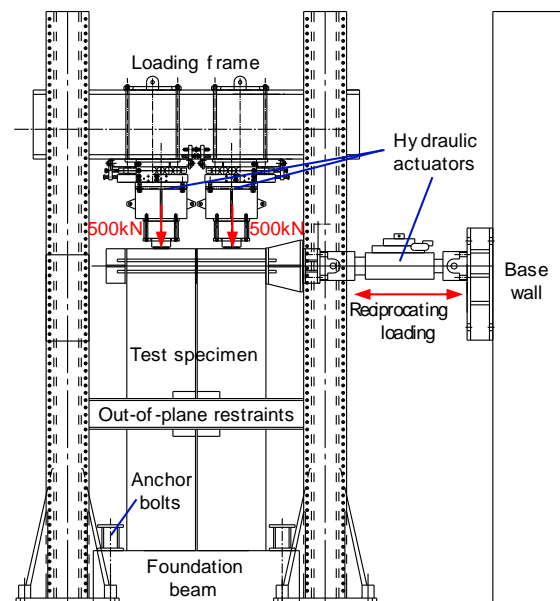


Fig. 6 Test setup

3.2 Test setup and loading scheme

Fig. 6 shows that the loading setup mainly included a loading frame and hydraulic actuators. The SSKW specimens were fixed at the bottom by jacks, pressing beams, and anchor bolts and were free at the top. Two vertical actuators were installed on the loading frame, providing an axial compressive force of 500 kN to each wall segment, equating to an axial force ratio of 0.2. Meanwhile, a horizontal actuator was used to exert a lateral reciprocal loading at the top of the specimens.

The loading history is shown in Fig. 7. Specimens were loaded to generate later drift amplitudes of 1/1000, 1/800, 1/500, 1/300, 1/200, 1/150, 1/100, 1/67, 1/50, and 1/40, and each amplitude was used in three cycles (Shen *et al.* 2017).

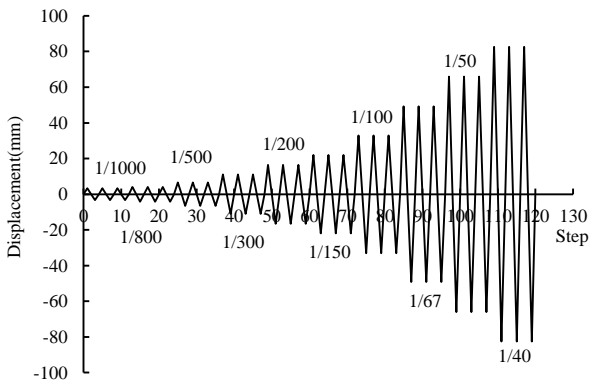


Fig. 7 Loading history

3.3 Measurement scheme

Many methods have been proposed on measuring the response of structures, including deformations, damage, etc. Yi *et al.* (2010, 2019) adopted GPS technology and real-time kinematic to realise full-scale measurement of the dynamic response of a suspension bridge, which exhibited outstanding accuracy and produced profound influence in monitoring. Ye *et al.* proposed imaged-based measurement and multi-point displacement monitoring along with multi-object tracking algorithms (2012, 2013, 2015a, b, 2016a, b, c), which showed considerable accuracy and high efficiency. In this study, the specimens were measured by displacement transducers strain gauges, and digital cameras. Fig. 8 shows that four displacement transducers, namely D1–D4, were mounted on the specimens, where D1 was used to measure the lateral displacement, d_1 , at the top of the specimens and D2 was used to measure the slippage, d_2 , of the foundation beam, so that the drift of the specimens could be calculated as

$$\Delta = \frac{d_1 - d_2}{h} \quad (3)$$

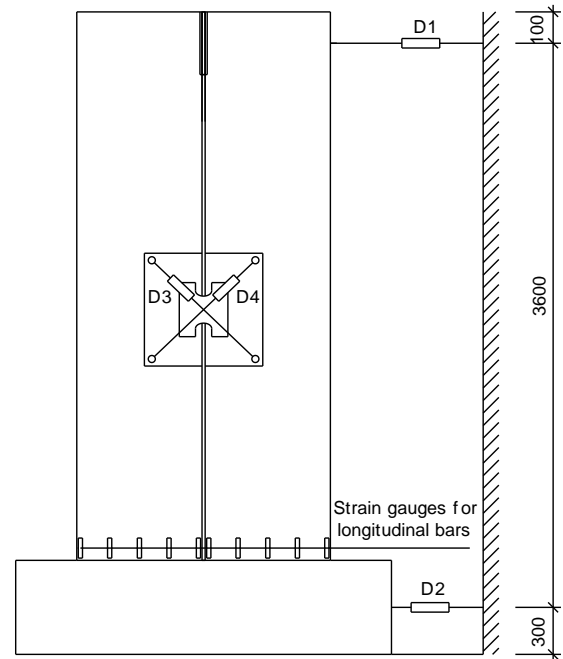
Here, h is the vertical distance between the loading point and foundation beam.

D3 and D4 were used to measure the diagonal deformations, d_3 and d_4 , of the SSKs, and the monitoring points were set at the corners of the embedded steel panels. Accordingly, the drift of SSKs can be calculated as

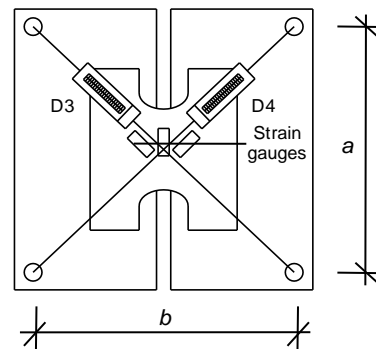
$$\theta = \frac{|d_3| + |d_4|}{\sqrt{a^2 + b^2}} \cdot \frac{a}{b} \quad (4)$$

where a and b are respectively the horizontal and vertical distances between the monitoring points.

The lateral restoring forces of the specimens were measured using a transducer, where a specimen was to be judged to have failed when the restoring force reduced to no more than 85% of its peak value (Shen *et al.* 2019a, b).



(a) Instrumentation for specimens



(b) Instrumentation for SSKs

Fig. 8 Layout of instrumentation system

4. Test results

4.1 Damage and failure mode

Figure 9 shows photographs of specimens A1 and A2 after testing. It is seen that the specimens failed mainly at the bottom of the wall segments, where the highest amounts of bending and strain were distributed. Consequently, the steel bars buckled and the concrete was crushed.

Fig. 10 shows photographs of the SSKs after testing. The SSK of A2 was fractured, whereas the SSK of A1 remained intact, despite A1 and A2 being equipped with SSKs of the same strength. This was due to n_s of E1 being 0.9, which resulted in a higher probability of fracturing of the rivets. Thus, the SSK of A1 failed in anchoring because it no longer deformed along with the lateral deformation of the wall segments. In comparison, E2, the anchoring component of the SSK in specimen A2, remained intact because of its high safety coefficient, meaning that the SSK

in A2 worked effectively throughout the loading test. With an increase in the loading drift, the deformation of the SSK gradually exceeded its capacity, and ultimately resulting in fracturing. There was not obvious out-of plane buckling observed in the energy dissipation plate of the SSK, additionally, the concrete cracking of A2 occurred earlier than that of A1 and with a larger cracking width, because E2 strengthened the wall segments in the local region, and a short column formed between the embedded anchoring components and the bottom of the shear wall, exhibiting the lack of deformation capacity and earlier cracking.

4.2 Lateral resistance and performance points

The hysteresis curves of the lateral restoring force versus the lateral displacement of the loading point for A1 and A2 are shown in Fig. 11 and the corresponding skeleton curves are shown in Fig. 12.



(a) A1



(b) A2

Fig. 9 Photographs of specimens after loading



(a) E1



(b) E2

Fig. 10 Hysteresis curves for specimens

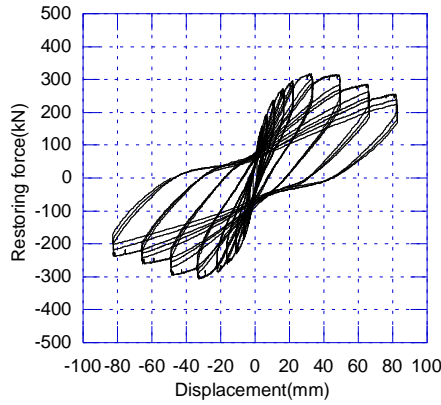
Table 1 Performance points for test specimens

Specimen	A1	A2
Initial stiffness (kN/mm)	40	44
Yield force of a specimen (kN)	183	198
Peak force (kN)	311	396
Yield drift of wall segments	1/470	1/485
Yield drift of SSK	1/800	1/820
Drift of peak force	1/100	1/50
Fracture drift of SSK	/	1/60
Fracture drift of embedded components	1/150	/
Ultimate drift of a specimen	1/41	1/44

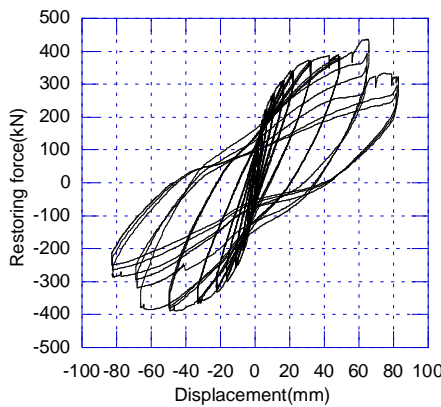
In general, A1 had lower lateral resistance than A2, whereas the restoring force of A2 rapidly declined after peaking. Detailed test results are listed in Table 1, where it is seen that the initial stiffness and yield force of A2 were respectively 44 kN/mm and 198 kN, values that are no more than 110% of those of A1. This indicates that the initial strengths of A1 and A2 were approximately similar. However, the peak force of A2 was 28% higher than that of A1, because the SSK of A1 failed in anchoring at a loading drift of 1/150, far before A1 reached the peak force.

Consequently, the linking of the two wall segments of A1 failed and the segments functioned independently with lower stiffness after the anchoring failure of the SSK. In comparison, the anchoring of the SSK in A2 remained intact and A2 thus functioned with an obviously higher lateral strength during the tests. However, after reaching a peak force at 1/50, A2 was quickly damaged at a drift of 1/44 and

the restoring force dropped by 25%. In comparison, the force of A1 reduced by 19% when the drift increased from 1/100 to 1/44. Notably, the declining slope was only 14% that of A2. This indicates that an n_s value as high as 2.1 for the embedded component E2 can lead to the rapid failure of specimen A2 after a peak force is reached.



(a) A1



(b) A2

Fig. 11 Hysteresis curves for specimens

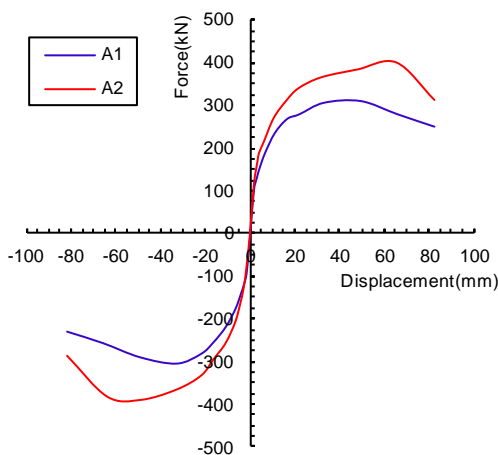


Fig. 12 Skeleton curves of specimens

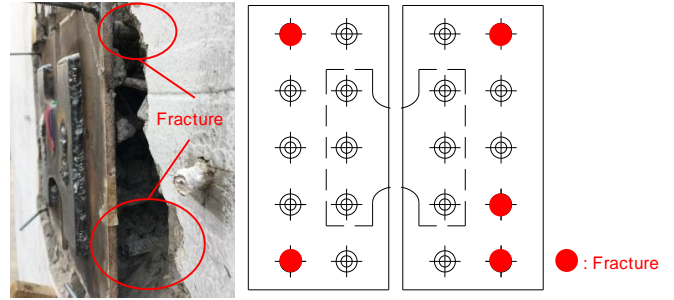


Fig. 13 Anchorage failure of E1

4.3 Performance of anchoring components

The embedded components E1 and E2 had different properties under loading. Specifically, E2 remained intact throughout the loading test whereas E1 was seriously damaged. Additionally, the maximum deformation drift of SSKs in A1 and A2 were 1/42 and 1/11, and the corresponding loading drift were 1/150 and 1/40, respectively. In Figure 13, the fractured rivets of E1 are marked with red points. It is observed that fracturing mainly occurred for the peripheral rivets located far from the stiffness center of E1, because each of them produced a higher shearing force under the rotating deformation of the SSKs, as shown in Fig. 2(a). Moreover, the anchoring failure was observed to be a vicious circle. As a rivet fractured, it could no longer bear the shear load. This put pressure on the other rivets, because they had to bear more shear force, which sped up the failure of anchoring. In conclusion, an n_s value as low as 0.9 is insufficient for anchoring because of the lack of the shear resistance of shearing rivets (Cui *et al.* 2018, Cui *et al.* 2019). Conversely, an n_s value as high as 2.1 can lead to the brittle failure of specimens. Therefore, from the results of the present study, an appropriate safety coefficient range between 1.3 and 1.7 is preliminarily assumed and to be validated in the future study.

5. Conclusions

A precast SSKW was developed alongside a design approach for anchoring components of SSKs. To obtain an appropriate range of safety coefficients n_s for design, two SSKW specimens with different strengths of SSK anchoring components were designed and loaded in quasi-static cyclic tests. The major findings of the study are as follows.

(1) The SSK of specimen A1 failed in anchoring at a loading drift of 1/150, indicating that an n_s value as low as 0.9 for the anchoring components is insufficient, because the failure process of anchoring is a vicious circle.

(2) The anchoring component E2 in specimen A2 remained intact. However, after reaching a peak force at a drift of 1/50, A2 was quickly damaged at a drift of 1/44, and its restoring force sharply decreased. This indicates that an n_s value as high as 2.1 for the embedded anchoring component E2 can lead to the brittle failure of specimens, giving rise to a short-column effect and a rapid decline in

lateral strength.

(3) The initial stiffness and yield force of A2 were only 10% higher than those of A1. However, the peak force was 28% higher for A2 than for A1. This indicates that n_s of the embedded components mainly affects the nonlinear properties of specimens, including the deformation ability after the peak force and the ultimate damage modes, instead of the initial status.

Acknowledgments

The authors are grateful for financial support from the National Key Research and Development Program of China (Project No. 2016YFC0701901), Natural Science Foundation of China (Grant Nos. 51778342 and 51578314), and Beijing Science and Technology Program (Grant No. Z161100001216015).

References

- Ameli, M.J., Brown, D.N., Parks, J.E. and Pantelides, C.P. (2016), "Column-to-footing connections using grouted splice sleeves", *ACI Struct. J.*, **113**(5), 1021-1030. DOI: 10.14359/51688755.
- Boafo, F.E., Kim, J.H. and Kim, J.T. (2016), "Performance of modular prefabricated architecture: case study-based review and future pathways", *Sustainability*, **8**(6), 558. DOI: 10.3390/su8060558.
- Cui, Y., Gao, X.Y. and Liu, H.T. and Yamada, S. (2018), "Experimental study on seismic behavior of roof joint", *Int. J. Steel Struct.*, **18**(4), 1373-1383. DOI: 10.1007/s13296-018-0142-7.
- Cui, Y., Liu, H.T. and Gao, X.Y. (2019) "Experimental study on seismic behavior of roof joint with different seismic isolation measure", *Earthq. Eng. Eng. Vib.*, **39**(1), 180-188. (in Chinese)
- Deng, K.L., Pan, P., Wang, H.S. and Shen, S.D. (2017), "Experimental study on slotted RC wall with steel energy dissipation links for seismic protection of buildings", *Eng. Struct.*, **145**, 1-11. DOI: 10.1016/j.engstruct.2017.05.006.
- El-Tawil, S., Harries, K.A., Fortney, P.J., Shahrooz, B.M. and Kurama, Y. (2010) Seismic design of hybrid coupled wall systems: state of the art. *J. Struct. Eng.*, **136**(7), 755-769. DOI: 10.1061/(ASCE)ST.1943-541X.0000186.
- Fintel, M. (1977), "Performance of precast concrete structures during rumanian earthquake of March 4", *PCI J.*, **22**(2), 10-15.
- Fintel, M. (1995), "Performance of buildings with shear walls in earthquakes of the last thirty years", *PCI J.*, **40**(3), 62-80.
- Ghosh, S.K. (1995), "Observations on the performance of structures in the Kobe Earthquake of January 17", *PCI J.*, **40**(2), 14-22.
- Guo, W., Zhai, Z.P., Cui, Y. Yu, Z.W. and Wu, X.L. (2019), "Seismic performance assessment of low-rise precast wall panel structure with bolt connections", *Eng. Struct.*, **181**, 562-578. DOI: 10.1016/j.engstruct.2018.12.060.
- Haber, Z.B. Saiidi, M.S. and Sanders D.H. (2014), "Seismic performance of precast columns with mechanically spliced column-footing connections", *ACI Struct. J.*, **111** (3), 639-50.
- Henin, E. and Morcou, G. (2015), "Non-proprietary bar splice sleeve for precast concrete construction", *Eng. Struct.*, **83**, 154-162. DOI: 10.1016/j.engstruct.2014.10.045.
- Khaled, A.S., Sami, H.R. and Robert, W.D. (1995), "Horizontal connections for precast concrete shear walls subjected to cyclic deformations Part 2: Prestressed connections", *PCI J.*, **40**(5), 82-96. DOI: 10.15554/pci.09011995.82.96.
- Lin, F. and Wu, X.B. (2016), "Effect of sleeve length on deformation properties of grouted splices", *Gradev.*, **69**(7), 537-546. DOI: 10.14256/JCE.1553.2016.
- Ling, J.H., Abd Rahman, A.B., Ibrahim, I.S. and Hamid, Z.A. (2016), "Tensile capacity of grouted splice sleeves", *Eng. Struct.*, **111**, 285-296. DOI: 10.1016/j.engstruct.2015.12.023.
- Ling, J.H., Abd Rahman, A.B., Ibrahim, I.S. and Hamid, Z.A. (2017), "An experimental study of welded bar sleeve wall panel connection under tensile, shear, and flexural loads", *Int. J. Concrete Struct. Mater.*, **11**(3), 525-540. DOI: 10.1007/s40069-017-0202-y.
- PRC National Standard (GB 50017-2017). (2017), "Standard for design of steel structures", Beijing, China, Ministry of Housing and Urban-Rural Construction of the People's Republic of China Press. (in Chinese)
- Scanlon, A., Kianoush, M.R. (1988), "Behavior of large panel precast coupled wall systems subjected to earthquake loading", *PCI J.*, **33** (5), 124-151.
- Smith, B.J., Kurama, Y.C. and McGinnis, M.J. (2007), "Design and measured behavior of a hybrid precast concrete wall specimen for seismic regions", *J. Struct. Eng.*, **137** (10), 58-79. DOI: 10.1061/(ASCE)ST.1943-541X.0000327.
- Sritharan, S., Aaleti, S., Henry, R.S., Liu, K.Y. and Tsai, K.C. (2015), "Precast concrete wall with end columns (PreWEC) for earthquake resistant design", *Earthq. Eng. Struct. D.*, **44**, 2075-2092. DOI: 10.1002/eqe.2576.
- Shen, S.D., Pan, P., Sun, J.B., Gong, R.H., Wang, H.S. and Li, W. (2017), "Development of a double-sliding friction damper (DSFD)", *Smart. Struct. Syst.*, **20**(2): 151-162. DOI: 10.12989/sss.2017.20.2.151.
- Shen, S.D., Cui, Y., Pan, P., Gong, R.H., Miao, Q.S. and Li, W.F. (2019a), "Experimental study of RC prefabricated shear walls with shear keys affected by a slotted floor slab", *J. Aerosp. Eng.*, **32**(3), 04019013. DOI: 10.1061/(ASCE)AS.1943-5525.0001000.
- Shen, S.D., Pan, P., Miao, Q.S., Li, W.F. and Gong, R.H. (2019b), "Behaviour of wall segments and floor slabs in precast reinforced concrete shear walls assembled using steel shear keys (SSKW)", *Struct. Control. Health Monit.*, **26**: e2418.
- VanGeem, M. (2006), "Achieving sustainability with precast concrete", *PCI J.*, **51** (1), 42-61. DOI: 10.15554/pci.01012006.42.61.
- Wu, D.Y., Liang, S.T., Guo, Z.X., Zhu, X.J. and Fu Q. (2016), "The development and experimental test of a new pore-forming grouted precast shear wall connector", *J. Civ. Eng.*, **20**(4), 1462-1472. DOI: 10.1007/s12205-015-0071-3.
- Yi, T.H., Li, H.N. and Gu, M. (2010), "Full-scale measurement of dynamic response of a suspension bridge subjected to environmental loads using GPS technology", *Sci. China-Technol. Sci.*, **53**(2): 469-479. DOI: 10.1007/s11431-010-0051-2.
- Yi, T.H., Yao, X.J., Qu, C.X. and Li, H.N. (2019), "Clustering number determination for sparse component analysis during output-only modal identification", *J. Eng. Mech.*, **145**(1): 04018122. DOI: 10.1061/(asce)em.1943-7889.0001557.
- Ye, X.W., Ni, Y.Q., Wong, K.Y. and Ko, J.M. (2012), "Statistical analysis of stress spectra for fatigue life assessment of steel bridges with structural health monitoring data", *Eng. Struct.*, **45**, 166-176. DOI: 10.1016/j.engstruct.2012.06.016.
- Ye, X.W., Ni, Y.Q., Wai, T.T., Wong, K.Y., Zhang, X.M. and Xu, F. (2013), "A vision-based system for dynamic displacement measurement of long-span bridges: algorithm and verification", *Smart. Struct. Syst.*, **12**(3-4), 363-379. https://doi.org/10.12989/sss.2013.12.3_4.363.
- Ye, X.W., Yi, T.H., Wen, C. and Su, Y.H. (2015a), "Reliability-based assessment of steel bridge deck using a mesh-insensitive structural stress method", *Smart. Struct. Syst.*, **16**(2), 367-382. <https://doi.org/10.12989/sss.2015.16.2.367>.

- Ye, X.W., Yi, T.H., Dong, C.Z., Liu, T. and Bai, H. (2015b), "Multi-point displacement monitoring of bridges using a vision-based approach", *Wind Struct.*, **20**(2), 315-326. <https://doi.org/10.12989/was.2015.20.2.315>.
- Ye, X.W., Dong, C.Z. and Liu, T. (2016a), "Image-based structural dynamic displacement measurement using different multi-object tracking algorithms", *Smart. Struct. Syst.*, **17**(6), 935-956. <https://doi.org/10.12989/sss.2016.17.6.935>.
- Ye, X.W., Su, Y.H., Xi, P.S., Chen, B. and Han, J.P. (2016b), "Statistical analysis and probabilistic modeling of WIM monitoring data of an instrumented arch bridge", *Smart. Struct. Syst.*, **17**(6), 1087-1105. <https://doi.org/10.12989/sss.2016.17.6.1087>.
- Ye, X.W., Yi, T.H., Dong, C.Z. and Liu, T. (2016c), "Vision-based structural displacement measurement: system performance evaluation and influence factor analysis", *Measurement*, **88**, 372-384. DOI: 10.1016/j.measurement.2016.01.024.
- Zhu, Z.F. and Guo, Z.X. (2018), "Reversed cyclic loading test on emulative hybrid precast concrete shear walls under different vertical loads", *J. Civ. Eng.*, **22**(11), 4364-4372. DOI: 10.1007/s12205-018-0736-9.